Perturbed eigenvalue problem with the Davidon-Fletcher-Powell quasi-Newton approach for damage detection of fixed-fixed beams

Chun Nam Wong, Hong-Zhong Huang, Jingqi Xiong, Tianyou Hu and Hua Long Lan

Mathematics and Mechanics of Solids 2011 16: 228 originally published online 13 January 2011
DOI: 10.1177/1081286510382820

Article

MMS

Mathematics and Mechanics of Solids
16(2): 228–247

DOI: 10.1177/1081286510382820
mms.sagepub.com

SAGE

Perturbed eigenvalue problem with the Davidon–Fletcher–Powell quasi-Newton approach for damage detection of fixed–fixed beams

Chun Nam Wong, Hong-Zhong Huang, Jingqi Xiong, Tianyou Hu
School of Mechatronic Engineering, University of Electronic Science and Technology of China, P.R. of China

Hua Long Lan
Jinchuan Group Ltd., P.R. of China

Received 1 April 2010; accepted 21 July 2010

Abstract
A damage detection method is formulated to estimate damage location and extent from non-*k*th perturbation terms of a specific set of eigenvectors and eigenvalues. The perturbed eigenvalue problem is established from the perturbations of stiffness matrix, eigenvector, and eigenvalue. Then stiffness parameters are estimated from this equation using the Davidon–Fletcher–Powell quasi-Newton approach. The optimization algorithm is iterative, and its process is monitored by *d*-norm and *t*-norm indicators. A fixed–fixed beam with an odd number of elements is used as a test structure to investigate the applicability of the method. In a five elements beam, *t*-norm convergences of the second-order algorithm are more effective for small and large-percentage damages. In medium-percentage damages, convergences of the first-order algorithm are faster for both indicators. Convergences of the general-order perturbation method are more effective for small and medium-percentage damages. Meanwhile, convergences of this method are slightly more effective in large-percentage damages. For seven elements medium-percentage damage and nine elements small-percentage damage, the second-order algorithm converges faster to the *t*-norm indicator. It is proven that convergence rate increases with the order of the algorithm.

Keywords
damage detection, fixed–fixed beam, Davidon–Fletcher–Powell quasi-Newton, non-*k*th coefficient, perturbed eigenvalue problem

1. Introduction

Perturbation analysis has been applied to various design and research areas, including parameter identifications, robust control systems, approximation of system response to changes in system parameters, assessment of design changes on system performance, analysis of structural systems with random parameters, and this application of damage detection using vibration diagnostics. Different researchers developed perturbation

Corresponding author:
Chun Nam Wong, Associate Professor, School of Mechanical, Electronic and Industrial Engineering, University of Electronic Science & Technology of China, Chengdu, Sichuan 610054, People's Republic of China.
Email: znhuang@uestc.edu.cn

approaches to deal with systems with distinctive eigenparameter features. They consisted of distinct eigenvalues, repeated eigenvalues, and closely spaced modes. Wilkenson [1] and Wong et al. [2, 3] derived the perturbation equation for damage detection of structural systems with distinct eigenvalues. Chen [4] and Hu [5] developed the perturbation equation to treat perturbed modes with a repeated eigenvalue, and Chen et al. [6] investigated the parameter changes in a vibration system with closely spaced eigenvalues.

In the theoretical design of structures, Wanxie and Gengdong [7] used the stationary nature of the Rayleigh quotient for second-order sensitivity analysis of multimodal eigenvalues. The results were applied to formulate a sequential quadratic programming approach for solving the problems of multimodal optimal design of structures. In their work, the Taylor's series expansions of the stiffness and mass matrices are presented. Wicher and Nalecz [8] presented a method for determining the second-order sensitivity matrix and logarithmic sensitivity functions in the frequency domain. A definition of the second-order logarithmic sensitivity function was proposed. A second-order perturbation method was developed by Ryland and Meirovitch [9] for the response of perturbed, undamped, non-gyroscopic dynamic systems where the eigenparameter perturbation arose from the small changes in system mass and stiffness parameters. Kan and Chopra [10, 11] derived the second-order perturbation analysis of a torsionally coupled building. However, the analysis was given based on the perturbation of a single parameter. A similar analysis was given by Tsicnias and Hutchinson [12].

An innovative part of this work is to derive the generalized perturbation coefficients where they can be applied to damage detection of common engineering systems. For the previous approach [2], the perturbed orthonormal equation is generated from the perturbation of eigenvectors and eigenvalues to obtain the kth perturbation coefficients. By eliminating these coefficients, efforts are made to utilize only the non-kth coefficients in the damage detection algorithms. Moreover, perturbation coefficients are constructed from the basic vectors of all used eigenvectors and their coefficients. Here the technique developed aims to evaluate generalized order terms explicitly, so that the generalized order perturbation coefficients can be constructed in sequential order. A quasi-Newton algorithm for large-scale optimization of perturbed eigenparameters is established. The algorithm makes use of inverse Hessian matrix and the gradient of the objective function, which is composed of weighted perturbation residuals. Meanwhile, the inverse Hessian matrix generated is based on the Davidon–Fletcher–Powell (DFP) formulation. This method is applicable to damage detection in different industries, such as aeronautical system, electrical transmission facilities [13], and gas turbine components. In addition, it can be applied to civilian structures, such as buildings and bridges.

2. Establishment of the perturbed eigenvalue problem

We derive here the perturbation of the eigenvalues and eigenvectors in the system equations from the eigenvalue problem. Consider here an original structural system with distinct eigenvalues; its eigenvalue problem before the estimation is

$$K\overline{\phi}^k = \lambda^k M\overline{\phi}^k, \tag{1}$$

where K, M are its system stiffness and mass matrices, respectively, and λ^k, $\overline{\phi}^k$ are its kth eigenvalue and eigenvector, respectively. The eigenvalue problem of the damaged structure is

$$K_d\overline{\phi}_d^k = \lambda_d^k M\overline{\phi}_d^k, \tag{2}$$

where K_d is its system stiffness matrix, and λ_d^k, $\overline{\phi}_d^k$ are its kth eigenvalue and eigenvector, respectively. Assuming K is a first-order function of G_d, higher-order perturbations of K with respect to the stiffness parameter G_d vanish. Using the first-order perturbation equation, the matrix K_d is related to K by

$$K_d = K + \sum_{d=1}^{m} \frac{\partial K}{\partial G_d}\delta G_d. \tag{3}$$

The kth eigenvalue and eigenvector of the damaged structure are related to those of the original structure through the perturbation expansions:

$$\lambda_d^k = \lambda^k + \sum_{d=1}^{m} \lambda_{(1)d}^k \delta G_d + \sum_{d=1}^{m}\sum_{e=1}^{m} \lambda_{(2)de}^k \delta G_d \delta G_e + \cdots + \underbrace{\sum_{d=1}^{m}\sum_{e=1}^{m}\cdots\sum_{z=1}^{m}}_{p \text{ summations}} \lambda_{(p)de\ldots z}^k \delta G_d \delta G_e \ldots \delta G_z + \varepsilon_\lambda^k, \quad (4)$$

$$\overline{\phi}_d^k = \overline{\phi}^k + \sum_{d=1}^{m}\sum_{\substack{a=1\\a\neq k}}^{n} P_{(1)da}^k \overline{\phi}^a \delta G_d + \sum_{d=1}^{m}\sum_{e=1}^{m}\sum_{\substack{b=1\\b\neq k}}^{n} P_{(2)deb}^k \overline{\phi}^b \delta G_d \delta G_e + \ldots$$
$$+ \sum_{d=1}^{m}\sum_{e=1}^{m}\cdots\sum_{z=1}^{m}\sum_{\substack{r=1\\r\neq k}}^{n} P_{(p)de\ldots zr}^k \overline{\phi}^r \delta G_d \delta G_e \ldots \delta G_z + \cdots + \overline{\varepsilon}_\phi^k, \quad (5)$$

where $\lambda_{(1)d}^k$, $\lambda_{(2)de}^k$, and $\lambda_{(p)de\ldots z}^k$ are the coefficients of the first-, second-, and pth order perturbation coefficients of the eigenvalue. $P_{(1)da}^k$, $P_{(2)deb}^k$, and $P_{(p)de\ldots zr}^k$ are the first-, second-, and pth order perturbation coefficients of the first-, second-, and pth order of the eigenvector. ε_λ^k and $\overline{\varepsilon}_\phi^k$ are the residuals of order p+1. In these summation series, running indexes $d, e, \ldots, z = 1, 2, \ldots, m$. Now we substitute these perturbed forms of $\lambda_d^k, \overline{\phi}_d^k$ and K_d into Equation (2):

$$\left\{K + \sum_{i=1}^{m} \frac{\partial K}{\partial G_i}\delta G_i\right\}\left\{\overline{\phi}^k + \sum_{i=1}^{m}\sum_{\substack{a=1\\a\neq k}}^{n} P_{(1)ia}^k \overline{\phi}^a \delta G_i + \sum_{i=1}^{m}\sum_{j=1}^{m}\sum_{\substack{b=1\\b\neq k}}^{n} P_{(2)ijb}^k \overline{\phi}^b \delta G_i \delta G_j + \ldots\right.$$
$$\left. + \sum_{i=1}^{m}\sum_{j=1}^{m}\cdots\sum_{t=1}^{m}\sum_{\substack{r=1\\r\neq k}}^{n} P_{(p)ij\ldots tr}^k \overline{\phi}^r \delta G_i \delta G_j \ldots \delta G_t + \ldots\right\}$$
$$= \left\{\lambda^k + \sum_{i=1}^{m} \lambda_{(1)i}^k \delta G_i + \sum_{i=1}^{m}\sum_{j=1}^{m} \lambda_{(2)ij}^k \delta G_i \delta G_j + \cdots + \sum_{i=1}^{m}\sum_{j=1}^{m}\cdots\sum_{t=1}^{m} \lambda_{(p)ij\ldots t}^k \delta G_i \delta G_j \ldots \delta G_t + \ldots\right\}$$
$$M\left\{\overline{\phi}^k + \sum_{i=1}^{m}\sum_{\substack{a=1\\a\neq k}}^{n} P_{(1)ia}^k \overline{\phi}^a \delta G_i + \sum_{i=1}^{m}\sum_{j=1}^{m}\sum_{\substack{b=1\\b\neq k}}^{n} P_{(2)ijb}^k \overline{\phi}^b \delta G_i \delta G_j + \ldots\right.$$
$$\left. + \sum_{i=1}^{m}\sum_{j=1}^{m}\cdots\sum_{t=1}^{m}\sum_{\substack{r=1\\r\neq k}}^{n} P_{(p)ij\ldots tr}^k \overline{\phi}^r \delta G_i \delta G_j \ldots \delta G_t + \ldots\right\}. \quad (6)$$

This is the perturbed eigenvalue problem of the damaged structure. Different order perturbation coefficients in the equation can be derived by equating the coefficients of like-order terms of δG_d. Equating the coefficients of the δG_d (d=1, 2, …, m) terms yields

$$K\sum_{\substack{a=1\\a\neq k}}^{n} P_{(1)da}^k \overline{\phi}^a + \frac{\partial K}{\partial G_d}\overline{\phi}^k = \lambda^k M \sum_{\substack{a=1\\a\neq k}}^{n} P_{(1)da}^k \overline{\phi}^a + \lambda_{(1)d}^k \mathrm{M}\overline{\phi}^k. \quad (7)$$

To obtain the eigenvalue coefficients by premultiplying this equation by $\overline{\phi}^{kT}$, one can make use of Equation (1) and the orthonormal relation to yield

$$\lambda_{(1)d}^k = \overline{\phi}^{kT} \frac{\partial K}{\partial G_d}\overline{\phi}^k. \quad (8)$$

On the other hand, the eigenvector coefficients can be obtained by premultiplying Equation (7) by $\overline{\phi}^{gT}$ where $g \neq k$. We get

$$\sum_{\substack{a=1\\a\neq k}}^{n} P^k_{(1)da}\overline{\phi}^{gT}K\overline{\phi}^{a} + \overline{\phi}^{gT}\frac{\partial K}{\partial G_d}\overline{\phi}^{k} = \lambda^k \sum_{\substack{a=1\\a\neq k}}^{n} P^k_{(1)da}\overline{\phi}^{gT}M\overline{\phi}^{a} + \lambda^k_{(1)d}\overline{\phi}^{gT}M\overline{\phi}^{k}. \tag{9}$$

Using Equation (1) and the orthonormal relations, we get $K\overline{\phi}^{g} = \lambda^g M\overline{\phi}^{g}$, resulting in

$$P^k_{(1)dg} = \frac{1}{\lambda^k - \lambda^g}\left\{\overline{\phi}^{gT}\frac{\partial K}{\partial G_d}\overline{\phi}^{k}\right\}. \tag{10}$$

Equating the coefficients of the $\delta G_d \delta G_e (d, e = 1, 2, \ldots, m)$ terms in the perturbed eigenvalue problem of the damaged structure, one can obtain

$$\begin{aligned}
&\frac{1}{\mathbf{R}^1_{de}!}K\sum_{\substack{b=1\\b\neq k}}^{n} P^k_{(2)deb}\overline{\phi}^{b} + \frac{1}{\mathbf{R}^1_{de}!}K\sum_{\substack{b=1\\b\neq k}}^{n} P^k_{(2)edb}\overline{\phi}^{b} + \frac{1}{1+\tau^e_d}\left[\frac{\partial K}{\partial G_d}\sum_{\substack{a=1\\a\neq k}}^{n} P^k_{(1)ea}\overline{\phi}^{a}\right] + \frac{1}{1+\tau^d_e}\left[\frac{\partial K}{\partial G_e}\sum_{\substack{a=1\\a\neq k}}^{n} P^k_{(1)da}\overline{\phi}^{a}\right] + \\
&= \frac{1}{\mathbf{R}^1_{de}!}\lambda^k M\sum_{\substack{b=1\\b\neq k}}^{n} P^k_{(2)deb}\overline{\phi}^{b} + \frac{1}{\mathbf{R}^1_{de}!}\lambda^k M\sum_{\substack{b=1\\b\neq k}}^{n} P^k_{(2)edb}\overline{\phi}^{b} + \frac{1}{1+\tau^e_d}\left[\lambda^k_{(1)d}M\sum_{\substack{a=1\\a\neq k}}^{n} P^k_{(1)ea}\overline{\phi}^{a}\right] \\
&\quad \frac{1}{1+\tau^d_e}\left[\lambda^k_{(1)e}M\sum_{\substack{a=1\\a\neq k}}^{n} P^k_{(1)da}\overline{\phi}^{a}\right] + \frac{1}{\mathbf{R}^1_{de}!}\lambda^k_{(2)de}M\overline{\phi}^{k} + \frac{1}{\mathbf{R}^1_{de}!}\lambda^k_{(2)ed}M\overline{\phi}^{k},
\end{aligned} \tag{11}$$

where τ^e_d is the generalized Kronecker delta defined by

$$\tau^e_d = \begin{cases} 1, & \text{if } d = e \\ 0, & \text{if } d \neq e \end{cases}. \tag{12}$$

The superscript in $\mathbf{R}^1_{de}$ denotes the number of repeated indexes, d and e, in the eigenvalue and eigenvector coefficients, and $\mathbf{R}^{1!}_{de}$ is the number of all possible permutations of these indexes. If d and e are repeated $\mathbf{R}^1_{de}! = 2!$, otherwise $\mathbf{R}^1_{de}! = 0!$. Consider the eigenvalue coefficients by premultiplying Equation (2) by $\overline{\phi}^{kT}$, and through the use of orthonormal relations, generalized Kronecker deltas, and permutation numbers, they are reduced to

$$\lambda^k_{(2)DE} = \mathbf{R}^1_{de}!\left(\frac{1}{1+\tau^e_d}\sum_{\substack{a=1\\a\neq k}}^{n} P^k_{(1)ea}\overline{\phi}^{kT}\frac{\partial K}{\partial G_d}\overline{\phi}^{a} + \frac{1}{1+\tau^d_e}\sum_{\substack{a=1\\a\neq k}}^{n} P^k_{(1)da}\overline{\phi}^{kT}\frac{\partial K}{\partial G_e}\overline{\phi}^{a}\right), \tag{13}$$

where $\lambda^k_{(2)DE}$ denotes all combination of $\lambda^k_{(2)de}$, i.e.$\lambda^k_{(2)DE} = \lambda^k_{(2)de} + \lambda^k_{(2)ed}$. Note that the upper case indexes in the subscript of the coefficient indicate that the orders of the indexes are not essential. When the second-order eigenvalue coefficient is symmetric, $\lambda^k_{(2)DE} = 2!\lambda^k_{(2)de}$. Equation (13) can be rewritten as

$$\lambda^k_{(2)de} = \frac{\mathbf{R}^1_{de}!}{2!}\left(\frac{1}{1+\tau^e_d}\sum_{\substack{a=1\\a\neq k}}^{n} P^k_{(1)ea}\overline{\phi}^{kT}\frac{\partial K}{\partial G_d}\overline{\phi}^{a} + \frac{1}{1+\tau^d_e}\sum_{\substack{a=1\\a\neq k}}^{n} P^k_{(1)da}\overline{\phi}^{kT}\frac{\partial K}{\partial G_e}\overline{\phi}^{a}\right). \tag{14}$$

Consider the eigenvector coefficients by premultiplying Equation (2) by $\overline{\phi}^{hT}$, where $h \neq k$. Through the use of Equation (1), and the orthonormal relations, they are reduced to

$$\frac{1}{\mathbf{R}^1_{de}!}\lambda^h P^k_{(2)deh} + \frac{1}{\mathbf{R}^1_{de}!}\lambda^h P^k_{(2)edh} + \frac{1}{1+\tau^e_d}\sum_{\substack{a=1\\a\neq k}}^{n} P^k_{(1)ea}\overline{\phi}^{hT}\frac{\partial \mathbf{K}}{\partial G_d}\overline{\phi}^a + \frac{1}{1+\tau^d_e}\sum_{\substack{a=1\\a\neq k}}^{n} P^k_{(1)da}\overline{\phi}^{hT}\frac{\partial \mathbf{K}}{\partial G_e}\overline{\phi}^a$$
$$= \frac{1}{\mathbf{R}^1_{de}!}\lambda^k P^k_{(2)deh} + \frac{1}{\mathbf{R}^1_{de}!}\lambda^k P^k_{(2)edh} + \frac{1}{1+\tau^e_d}\lambda^k_{(1)d}P^k_{(1)eh} + \frac{1}{1+\tau^d_e}\lambda^k_{(1)e}P^k_{(1)dh}. \tag{15}$$

Simplifying this equation, one can obtain

$$P^k_{(2)DEh} = \frac{\mathbf{R}^1_{de}!}{\lambda^k-\lambda^h}\left(\frac{1}{1+\tau^e_d}\sum_{\substack{a=1\\a\neq k}}^{n} P^k_{(1)ea}\overline{\phi}^{hT}\frac{\partial K}{\partial G_d}\overline{\phi}^a + \frac{1}{1+\tau^d_e}\sum_{\substack{a=1\\a\neq k}}^{n} P^k_{(1)da}\overline{\phi}^{hT}\frac{\partial K}{\partial G_e}\overline{\phi}^a\right.$$
$$\left. -\frac{1}{1+\tau^e_d}\lambda^k_{(1)d}P^k_{(1)eh} - \frac{1}{1+\tau^d_e}\lambda^k_{(1)e}P^k_{(1)dh}\right), \tag{16}$$

where $P^k_{(2)DE}$ denotes all combinations of $P^k_{(2)de}$, i.e. $P^k_{(2)DE} = P^k_{(2)de} + P^k_{(2)ed}$. When the eigenvector coefficient is symmetric, one has $P^k_{(2)de} = P^k_{(2)ed}$. Therefore, Equation (16) can be rewritten as

$$P^k_{(2)deh} = \frac{\mathbf{R}^1_{de}!}{2!\left(\lambda^k-\lambda^h\right)}\left(\frac{1}{1+\tau^e_d}\sum_{\substack{a=1\\a\neq k}}^{n} P^k_{(1)ea}\overline{\phi}^{hT}\frac{\partial K}{\partial G_d}\overline{\phi}^a + \frac{1}{1+\tau^d_e}\sum_{\substack{a=1\\a\neq k}}^{n} P^k_{(1)da}\overline{\phi}^{hT}\frac{\partial K}{\partial G_e}\overline{\phi}^a\right.$$
$$\left. -\frac{1}{1+\tau^e_d}\lambda^k_{(1)d}P^k_{(1)eh} - \frac{1}{1+\tau^d_e}\lambda^k_{(1)e}P^k_{(1)dh}\right). \tag{17}$$

Now we can proceed to find the *pth* order eigenvalue and eigenvector coefficients. Considering the cases with $m \geq p$, equating the coefficients of the $\delta G_d \delta G_e \ldots \delta G_z$ ($d,e, \ldots, z = 1, 2, \ldots, m$) terms in perturbed eigenvalue problem results in

$$K\sum_{\substack{r=1\\r\neq k}}^{n}\frac{P^k_{(p)DE\ldots Zr}}{\mathbf{R}^1_{de\ldots z}!\mathbf{R}^2_{de\ldots z}!\ldots\mathbf{R}^{\alpha}_{de\ldots z}!}\overline{\phi}^r + \frac{1}{1+\tau^{EF\ldots Z}_d}\frac{\partial K}{\partial G_d}\sum_{\substack{q=1\\q\neq k}}^{n}\frac{P^k_{(p-1)EF\ldots Zq}}{\mathbf{R}^1_{ef\ldots z}!\mathbf{R}^2_{ef\ldots z}!\ldots\mathbf{R}^{\beta}_{ef\ldots z}!}\overline{\phi}^q$$
$$+\frac{1}{1+\tau^{DF\ldots Z}_e}\frac{\partial K}{\partial G_e}\sum_{\substack{q=1\\q\neq k}}^{n}\frac{P^k_{(p-1)DF\ldots Zq}}{\mathbf{R}^1_{df\ldots z}!\mathbf{R}^2_{df\ldots z}!\ldots\mathbf{R}^{\chi}_{df\ldots z}!}\overline{\phi}^q + \cdots + \frac{1}{1+\tau^{DE\ldots Y}_z}\frac{\partial K}{\partial G_z}\sum_{\substack{q=1\\q\neq k}}^{n}\frac{P^k_{(p-1)D\ldots XYq}}{\mathbf{R}^1_{d\ldots xy}!\mathbf{R}^2_{d\ldots xy}!\ldots\mathbf{R}^{\varphi}_{de\ldots xy}!}\overline{\phi}^q$$
$$=\lambda^k M\sum_{\substack{r=1\\r\neq k}}^{n}\frac{P^k_{(p)DE\ldots Zr}}{\mathbf{R}^1_{de\ldots z}!\mathbf{R}^2_{de\ldots z}!\ldots\mathbf{R}^{\alpha}_{de\ldots z}!}\overline{\phi}^r + \frac{\lambda^k_{(1)d}}{1+\tau^{EF\ldots Z}_d}M\sum_{\substack{q=1\\q\neq k}}^{n}\frac{P^k_{(p-1)EF\ldots Zq}}{\mathbf{R}^1_{ef\ldots z}!\mathbf{R}^2_{ef\ldots z}!\ldots\mathbf{R}^{\beta}_{ef\ldots z}!}\overline{\phi}^q$$
$$+\frac{\lambda^k_{(1)e}}{1+\tau^{DF\ldots Z}_e}M\sum_{\substack{q=1\\q\neq k}}^{n}\frac{P^k_{(p-1)DF\ldots Zq}}{\mathbf{R}^1_{df\ldots z}!\mathbf{R}^2_{df\ldots z}!\ldots\mathbf{R}^{\chi}_{df\ldots z}!}\overline{\phi}^q + \cdots + \frac{\lambda^k_{(1)z}}{1+\tau^{D\ldots XY}_z}M\sum_{\substack{q=1\\q\neq k}}^{n}\frac{P^k_{(p-1)D\ldots XYq}}{\mathbf{R}^1_{d\ldots xy}!\mathbf{R}^2_{d\ldots xy}!\ldots\mathbf{R}^{\varphi}_{d\ldots xy}!}\overline{\phi}^q$$
$$+\frac{\lambda^k_{(2)DE}}{\mathbf{R}^1_{de}!\left(1+\tau^{F\ldots YZ}_{DE}\right)}M\sum_{\substack{p=1\\p\neq k}}^{n}\frac{P^k_{(p-2)F\ldots YZp}}{\mathbf{R}^1_{f\ldots yz}!\mathbf{R}^2_{f\ldots yz}!\ldots\mathbf{R}^{\gamma}_{f\ldots yz}!}\overline{\phi}^p + \frac{\lambda^k_{(2)DF}}{\mathbf{R}^1_{df}!\left(1+\tau^{E\ldots YZ}_{DF}\right)}$$
$$M\sum_{\substack{p=1\\p\neq k}}^{n}\frac{P^k_{(p-2)E\ldots YZp}}{\mathbf{R}^1_{e\ldots yz}!\mathbf{R}^2_{e\ldots yz}!\ldots\mathbf{R}^{\eta}_{e\ldots yz}!}\overline{\phi}^p + \ldots$$

$$\frac{\lambda^k_{(2)DZ}}{\mathbf{R}^1_{dz}!\left(1+\tau^{E\ldots XY}_{DZ}\right)}M\sum_{\substack{p=1\\p\neq k}}^{n}\frac{P^k_{(p-2)E\ldots XYp}}{\mathbf{R}^1_{e\ldots xy}!\mathbf{R}^2_{e\ldots xy}!\ldots\mathbf{R}^{\kappa}_{e\ldots xy}!}\overline{\phi}^p+\frac{\lambda^k_{(2)EF}}{\mathbf{R}^1_{ef}!\left(1+\tau^{D\ldots YZ}_{EF}\right)}$$

$$M\sum_{\substack{p=1\\p\neq k}}^{n}\frac{P^k_{(p-2)D\ldots YZp}}{\mathbf{R}^1_{d\ldots yz}!\mathbf{R}^2_{d\ldots yz}!\ldots\mathbf{R}^{\mu}_{d\ldots yz}!}\overline{\phi}^p+\ldots$$

$$\frac{\lambda^k_{(2)EZ}}{\mathbf{R}^1_{ez}!\left(1+\tau^{D\ldots XY}_{EZ}\right)}M\sum_{\substack{p=1\\p\neq k}}^{n}\frac{P^k_{(p-2)D\ldots XYp}}{\mathbf{R}^1_{d\ldots xy}!\mathbf{R}^2_{d\ldots xy}!\ldots\mathbf{R}^{\nu}_{d\ldots xy}!}\overline{\phi}^p+\cdots+\frac{\lambda^k_{(2)YZ}}{\mathbf{R}^1_{yz}!\left(1+\tau^{DE\ldots X}_{YZ}\right)}$$

$$M\sum_{\substack{p=1\\p\neq k}}^{n}\frac{P^k_{(p-2)DE\ldots Xp}}{\mathbf{R}^1_{de\ldots x}!\mathbf{R}^2_{de\ldots x}!\ldots\mathbf{R}^{\varpi}_{de\ldots x}!}\overline{\phi}^p$$

$$+\cdots+\frac{\lambda^k_{(p-1)EF\ldots Z}}{\mathbf{R}^1_{ef\ldots z}!\mathbf{R}^2_{ef\ldots z}!\ldots\mathbf{R}^{\beta}_{ef\ldots z}!\left(1+\tau^{d}_{EF\ldots Z}\right)}M\sum_{\substack{a=1\\a\neq k}}^{n}P^k_{(1)da}\overline{\phi}^a$$

$$+\frac{\lambda^k_{(p-1)DF\ldots Z}}{\mathbf{R}^1_{df\ldots z}!\mathbf{R}^2_{df\ldots z}!\ldots\mathbf{R}^{\chi}_{df\ldots z}!\left(1+\tau^{\chi}_{DF\ldots Z}\right)}M\sum_{\substack{a=1\\a\neq k}}^{n}P^k_{(1)ea}\overline{\phi}^a$$

$$+\cdots+\frac{\lambda^k_{(p-1)DE\ldots Y}}{\mathbf{R}^1_{de\ldots y}!\mathbf{R}^2_{de\ldots y}!\ldots\mathbf{R}^{\varphi}_{de\ldots y}!\left(1+\tau^{z}_{DE\ldots Y}\right)}M\sum_{\substack{a=1\\a\neq k}}^{n}P^k_{(1)za}\overline{\phi}^a+\frac{\lambda^k_{(p)DE\ldots Z}}{\mathbf{R}^1_{de\ldots z}!\mathbf{R}^2_{de\ldots z}!\ldots\mathbf{R}^{\alpha}_{de\ldots z}!}M\overline{\phi}^k, \quad (18)$$

where the generalized Kronecker deltas, such as $\tau^{EF\ldots Z}_{d}$ and $\tau^{F\ldots YZ}_{DE}$, are defined by

$$\tau^{EF\ldots Z}_{d}=\begin{cases}1\,, & \text{if } d=e,f,\ldots, \text{ or } z\\ 0, & \text{if } d\neq e,f,\ldots, \text{ and } z\end{cases} \quad (19)$$

and

$$\tau^{F\ldots YZ}_{DE}=\begin{cases}1\,, & \text{if } d \text{ and } e \text{ appear in the indices in the superscript}\\ 0, & \text{if } d \text{ and } e \text{ do not appear in the indices in the superscript}\end{cases}, \quad (20)$$

respectively. Eigenvector and eigenvalue coefficients, such as $P^k_{(p)DE\ldots Zq}$ and $\lambda^k_{(p-1)EF\ldots Z}$, represent the sums of all terms of the forms $P^k_{(p)de\ldots z}$ and $\lambda^k_{(p-1)ef\ldots z}$, respectively, with different permutations of indexes $d,e,\ldots z$ and $e,f,\ldots,z$. The coefficients, such as $\mathbf{R}^1_{de\ldots z}$,$\mathbf{R}^2_{de\ldots z}$,…,$\mathbf{R}^{\alpha}_{de\ldots z}$, are the numbers of the first, second and last repeated indexes within indexes $d,e,\ldots,z$, respectively. Note that the upper case indexes in the sub- and superscripts of all the generalized Kronecker deltas in Equations (19) and (20) indicate that the orders of the indexes are not essential. Premultiplying Equation (18) by $\overline{\phi}^{kT}$ and using Equation (1) and the orthonormal relations in the resulting equation, one can obtain

$$\lambda^k_{(p)DE\ldots Z}=\mathbf{R}^1_{de\ldots n}!\mathbf{R}^2_{de\ldots n}!\ldots\mathbf{R}^{\alpha}_{de\ldots n}!\left(\frac{1}{1+\tau^{EF\ldots Z}_{d}}\sum_{\substack{q=1\\q\neq k}}^{n}\frac{P^k_{(p-1)EF\ldots Zq}}{\mathbf{R}^1_{ef\ldots z}!\mathbf{R}^2_{ef\ldots z}!\ldots\mathbf{R}^{\beta}_{ef\ldots z}!}\overline{\phi}^{kT}\frac{\partial K}{\partial G_d}\overline{\phi}^q+\frac{1}{1+\tau^{DF\ldots Z}_{e}}\right.$$

$$\left.+\sum_{\substack{q=1\\q\neq k}}^{n}\frac{P^k_{(p-1)DF\ldots Zq}}{\mathbf{R}^1_{df\ldots z}!\mathbf{R}^2_{df\ldots z}!\ldots\mathbf{R}^{\chi}_{df\ldots z}!}\overline{\phi}^{kT}\frac{\partial K}{\partial G_e}\overline{\phi}^q+\cdots+\frac{1}{1+\tau^{DE\ldots Y}_{z}}\sum_{\substack{q=1\\q\neq k}}^{n}\frac{P^k_{(p-1)DE\ldots Yq}}{\mathbf{R}^1_{de\ldots y}!\mathbf{R}^2_{de\ldots y}!\ldots\mathbf{R}^{\varphi}_{de\ldots y}!}\overline{\phi}^{kT}\frac{\partial K}{\partial G_z}\overline{\phi}^q\right), \quad (21)$$

where $\lambda^k_{(p)DE\ldots Z}$ denotes the summation of all combination of $\lambda^k_{(p)de\ldots z}$, i.e. $\lambda^k_{(p)DE\ldots Z} = \lambda^k_{(p)de\ldots z} + \lambda^k_{(p)ed\ldots z} + \cdots + \lambda^k_{(p)d\ldots yz}$. When the eigenparameter coefficients are symmetric, their total numbers are the factorial numbers of their orders, i.e. $\lambda^k_{(p)DE\ldots Z} = p!\lambda^k_{(p)de\ldots z}$. So the pth-order eigenvalue coefficient is reduced to

$$\lambda^k_{(p)de\ldots z} = \frac{\mathbf{R}^1_{de\ldots n}!\mathbf{R}^2_{de\ldots n}!\ldots\mathbf{R}^{\alpha}_{de\ldots n}!}{p!}\left(\frac{1}{1+\tau_d^{EF\ldots Z}}\sum_{\substack{q=1\\q\neq k}}^{n}\frac{(p-1)!P^k_{(p-1)ef\ldots zq}}{\mathbf{R}^1_{ef\ldots z}!\mathbf{R}^2_{ef\ldots z}!\ldots\mathbf{R}^{\beta}_{ef\ldots z}!}\overline{\phi}^{kT}\frac{\partial K}{\partial G_d}\overline{\phi}^{q} + \frac{1}{1+\tau_e^{DF\ldots Z}}\right.$$
$$\left.\sum_{\substack{q=1\\q\neq k}}^{n}\frac{(p-1)!P^k_{(p-1)df\ldots zq}}{\mathbf{R}^1_{df\ldots z}!\mathbf{R}^2_{df\ldots z}!\ldots\mathbf{R}^{\chi}_{df\ldots z}!}\overline{\phi}^{kT}\frac{\partial K}{\partial G_e}\overline{\phi}^{q} + \cdots + \frac{1}{1+\tau_z^{DE\ldots Y}}\sum_{\substack{q=1\\q\neq k}}^{n}\frac{(p-1)!P^k_{(p-1)de\ldots yq}}{\mathbf{R}^1_{de\ldots y}!\mathbf{R}^2_{de\ldots y}!\ldots\mathbf{R}^{\varphi}_{de\ldots y}!}\overline{\phi}^{kT}\frac{\partial K}{\partial G_z}\overline{\phi}^{q}\right). \quad (22)$$

Premultiplying Equation (18) by $\overline{\phi}^{wT}$, where $w \neq k$, and using Equation (1) and the orthonormal relations, yields the generalized order eigenvector coefficient

$$P^k_{(p)DE\ldots Zw} = \frac{\mathbf{R}^1_{de\ldots z}!\mathbf{R}^2_{de\ldots z}!\ldots\mathbf{R}^{x}_{de\ldots z}!}{\lambda^k-\lambda^w}\left[\frac{1}{1+\tau_d^{EF\ldots Z}}\sum_{\substack{q=1\\q\neq k}}^{n}\frac{P^k_{(p-1)EF\ldots Zq}}{\mathbf{R}^1_{ef\ldots z}!\mathbf{R}^2_{ef\ldots z}!\ldots\mathbf{R}^{\beta}_{ef\ldots z}!}\overline{\phi}^{wT}\frac{\partial K}{\partial G_d}\overline{\phi}^{q}\right.$$
$$+\frac{1}{1+\tau_e^{DF\ldots Z}}\sum_{\substack{q=1\\q\neq k}}^{n}\frac{P^k_{(p-1)DF\ldots Zq}}{\mathbf{R}^1_{df\ldots z}!\mathbf{R}^2_{df\ldots z}!\ldots\mathbf{R}^{\chi}_{df\ldots z}!}\overline{\phi}^{wT}\frac{\partial K}{\partial G_e}\overline{\phi}^{q}+\cdots+\frac{1}{1+\tau_z^{DE\ldots Y}}$$
$$\left.\sum_{\substack{q=1\\q\neq k}}^{n}\frac{P^k_{(p-1)DE\ldots Yq}}{\mathbf{R}^1_{de\ldots y}!\mathbf{R}^2_{de\ldots y}!\ldots\mathbf{R}^{\varphi}_{de\ldots y}!}\overline{\phi}^{wT}\frac{\partial K}{\partial G_z}\overline{\phi}^{q}\right.$$
$$-\frac{\lambda^k_{(1)d}}{1+\tau_d^{EF\ldots Z}}\frac{P^k_{(p-1)EF\ldots Zw}}{\mathbf{R}^1_{ef\ldots z}!\mathbf{R}^2_{ef\ldots z}!\ldots\mathbf{R}^{\beta}_{ef\ldots z}!}-\frac{\lambda^k_{(1)e}}{1+\tau_e^{DF\ldots Z}}\frac{P^k_{(p-1)DF\ldots Zw}}{\mathbf{R}^1_{df\ldots z}!\mathbf{R}^2_{df\ldots z}!\ldots\mathbf{R}^{\chi}_{df\ldots z}!}-\cdots-$$
$$\frac{\lambda^k_{(1)z}}{1+\tau_z^{D\ldots XY}}\frac{P^k_{(p-1)D\ldots XYw}}{\mathbf{R}^1_{d\ldots xy}!\mathbf{R}^2_{d\ldots xy}!\ldots\mathbf{R}^{\varphi}_{d\ldots xy}!}-\frac{\lambda^k_{(2)DE}}{\mathbf{R}^1_{de}!\left(1+\tau_{DE}^{F\ldots YZ}\right)}\frac{P^k_{(p-2)F\ldots YZw}}{\mathbf{R}^1_{f\ldots yz}!\mathbf{R}^2_{f\ldots yz}!\ldots\mathbf{R}^{\gamma}_{f\ldots yz}!}$$
$$-\frac{\lambda^k_{(2)DF}}{\mathbf{R}^1_{df}!\left(1+\tau_{DF}^{E\ldots MN}\right)}\frac{P^k_{(p-2)E\ldots MNw}}{\mathbf{R}^1_{e\ldots mn}!\mathbf{R}^2_{e\ldots mn}!\ldots\mathbf{R}^{\eta}_{e\ldots mn}!}-\cdots-\frac{\lambda^k_{(2)DN}}{\mathbf{R}^1_{dn}!\left(1+\tau_{DN}^{E\ldots LM}\right)}\frac{P^k_{(p-2)E\ldots LMw}}{\mathbf{R}^1_{e\ldots lm}!\mathbf{R}^2_{e\ldots lm}!\ldots\mathbf{R}^{\kappa}_{e\ldots lm}!}$$
$$-\frac{\lambda^k_{(2)EF}}{\mathbf{R}^1_{ef}!\left(1+\tau_{EF}^{D\ldots MN}\right)}\frac{P^k_{(p-2)D\ldots MNw}}{\mathbf{R}^1_{d\ldots mn}!\mathbf{R}^2_{d\ldots mn}!\ldots\mathbf{R}^{\mu}_{d\ldots mn}!}-\cdots-\frac{\lambda^k_{(2)EN}}{\mathbf{R}^1_{en}!\left(1+\tau_{EN}^{D\ldots LM}\right)}\frac{P^k_{(p-2)D\ldots LMw}}{\mathbf{R}^1_{d\ldots lm}!\mathbf{R}^2_{d\ldots lm}!\ldots\mathbf{R}^{\nu}_{d\ldots lm}!}$$
$$-\cdots-\frac{\lambda^k_{(2)MN}}{\mathbf{R}^1_{mn}!\left(1+\tau_{MN}^{DE\ldots L}\right)}\frac{P^k_{(p-2)DE\ldots Lw}}{\mathbf{R}^1_{de\ldots l}!\mathbf{R}^2_{de\ldots l}!\ldots\mathbf{R}^{\varpi}_{de\ldots l}!}-\cdots-$$
$$\frac{\lambda^k_{(p-1)EF\ldots N}}{\mathbf{R}^1_{ef\ldots n}!\mathbf{R}^2_{ef\ldots n}!\ldots\mathbf{R}^{\beta}_{ef\ldots n}!\left(1+\tau_{EF\ldots N}^{d}\right)}P^k_{(1)dw}-\frac{\lambda^k_{(p-1)DF\ldots N}}{\mathbf{R}^1_{df\ldots n}!\mathbf{R}^2_{df\ldots n}!\ldots\mathbf{R}^{\chi}_{df\ldots n}!\left(1+\tau_{DF\ldots N}^{e}\right)}P^k_{(1)ew}-\cdots-$$
$$\left.\frac{\lambda^k_{(p-1)DE\ldots M}}{\mathbf{R}^1_{de\ldots m}!\mathbf{R}^2_{de\ldots m}!\ldots\mathbf{R}^{\varphi}_{de\ldots m}!\left(1+\tau_{DE\ldots M}^{z}\right)}P^k_{(1)nw}\right]. \quad (23)$$

Now considering that the coefficients are symmetric, their total numbers are the factorial numbers of their orders. Therefore, the pth-order symmetric eigenvector coefficient can be rewritten as

$$
\begin{aligned}
P^k_{(p)de\ldots zw} = {} & \frac{\mathbf{R}^1_{de\ldots z}!\mathbf{R}^2_{de\ldots z}!\ldots\mathbf{R}^x_{de\ldots z}!}{p!\left(\lambda^k-\lambda^w\right)}\left[\frac{1}{1+\tau_d^{EF\ldots Z}}\sum_{\substack{q=1\\q\neq k}}^{n}\frac{(p-1)!P^k_{(p-1)ef\ldots zq}}{\mathbf{R}^1_{ef\ldots z}!\mathbf{R}^2_{ef\ldots z}!\ldots\mathbf{R}^\beta_{ef\ldots z}!}\overline{\phi}^{wT}\frac{\partial \mathrm{K}}{\partial G_d}\overline{\phi}^{q}\right.\\
& +\frac{1}{1+\tau_e^{DF\ldots Z}}\sum_{\substack{q=1\\q\neq k}}^{n}\frac{(p-1)!P^k_{(p-1)df\ldots zq}}{\mathbf{R}^1_{df\ldots z}!\mathbf{R}^2_{df\ldots z}!\ldots\mathbf{R}^\chi_{df\ldots z}!}\overline{\phi}^{wT}\frac{\partial K}{\partial G_e}\overline{\phi}^{q}+\cdots+\frac{1}{1+\tau_z^{DE\ldots Y}}\\
& \left.\sum_{\substack{q=1\\q\neq k}}^{n}\frac{(p-1)!P^k_{(p-1)de\ldots yq}}{\mathbf{R}^1_{de\ldots y}!\mathbf{R}^2_{de\ldots y}!\ldots\mathbf{R}^\varphi_{de\ldots y}!}\overline{\phi}^{wT}\frac{\partial K}{\partial G_z}\overline{\phi}^{q}\right.\\
& -\frac{\lambda^k_{(1)d}}{1+\tau_d^{EF\ldots Z}}\frac{(p-1)!P^k_{(p-1)ef\ldots zw}}{\mathbf{R}^1_{ef\ldots z}!\mathbf{R}^2_{ef\ldots z}!\ldots\mathbf{R}^\beta_{ef\ldots z}!}-\frac{\lambda^k_{(1)e}}{1+\tau_e^{DF\ldots Z}}\frac{(p-1)!P^k_{(p-1)df\ldots zw}}{\mathbf{R}^1_{df\ldots z}!\mathbf{R}^2_{df\ldots z}!\ldots\mathbf{R}^\chi_{df\ldots z}!}-\cdots-\\
& \frac{\lambda^k_{(1)z}}{1+\tau_n^{D\ldots XY}}\frac{(p-1)!P^k_{(p-1)d\ldots xyw}}{\mathbf{R}^1_{d\ldots xy}!\mathbf{R}^2_{d\ldots xy}!\ldots\mathbf{R}^\varphi_{d\ldots xy}!}-\frac{2!\lambda^k_{(2)de}}{\mathbf{R}^1_{de}!\left(1+\tau_{DE}^{F\ldots YZ}\right)}\frac{(p-2)!P^k_{(p-2)f\ldots yzw}}{\mathbf{R}^1_{f\ldots yz}!\mathbf{R}^2_{f\ldots yz}!\ldots\mathbf{R}^\gamma_{f\ldots yz}!}\\
& -\frac{2!\lambda^k_{(2)df}}{\mathbf{R}^1_{df}!\left(1+\tau_{DF}^{E\ldots MN}\right)}\frac{(p-2)!P^k_{(p-2)e\ldots mnw}}{\mathbf{R}^1_{e\ldots mn}!\mathbf{R}^2_{e\ldots mn}!\ldots\mathbf{R}^\eta_{e\ldots mn}!}-\cdots-\frac{2!\lambda^k_{(2)DN}}{\mathbf{R}^1_{dn}!\left(1+\tau_{DN}^{E\ldots LM}\right)}\frac{(p-2)!P^k_{(p-2)E\ldots LMw}}{\mathbf{R}^1_{e\ldots lm}!\mathbf{R}^2_{e\ldots lm}!\ldots\mathbf{R}^\kappa_{e\ldots lm}!}\\
& -\frac{2!\lambda^k_{(2)EF}}{\mathbf{R}^1_{ef}!\left(1+\tau_{EF}^{D\ldots MN}\right)}\frac{(p-2)!P^k_{(p-2)d\ldots mnw}}{\mathbf{R}^{\phi1}_{d\ldots mn}!\mathbf{R}^{\phi2}_{d\ldots mn}!\ldots\mathbf{R}^\mu_{d\ldots mn}!}-\cdots-\frac{2!\lambda^k_{(2)EN}}{\mathbf{R}^1_{en}!\left(1+\tau_{EN}^{D\ldots LM}\right)}\frac{(p-2)!P^k_{(p-2)D\ldots LMw}}{\mathbf{R}^1_{d\ldots lm}!\mathbf{R}^2_{d\ldots lm}!\ldots\mathbf{R}^\nu_{d\ldots lm}!}\\
& -\cdots-\frac{2!\lambda^k_{(2)MN}}{\mathbf{R}^1_{mn}!\left(1+\tau_{MN}^{DE\ldots L}\right)}\frac{(p-2)!P^k_{(p-2)DE\ldots Lw}}{\mathbf{R}^1_{de\ldots l}!\mathbf{R}^2_{de\ldots l}!\ldots\mathbf{R}^\varpi_{de\ldots l}!}-\cdots-\\
& \frac{(p-1)!\lambda^k_{(p-1)EF\ldots N}}{\mathbf{R}^1_{ef\ldots n}!\mathbf{R}^2_{ef\ldots n}!\ldots\mathbf{R}^\beta_{ef\ldots n}!\left(1+\tau^d_{EF\ldots N}\right)}P^k_{(1)dw}-\frac{(p-1)!\lambda^k_{(p-1)DF\ldots N}}{\mathbf{R}^1_{df\ldots n}!\mathbf{R}^2_{df\ldots n}!\ldots\mathbf{R}^\chi_{df\ldots n}!\left(1+\tau^e_{DF\ldots N}\right)}P^k_{(1)ew}-\cdots-\\
& \left.\frac{(p-1)!\lambda^k_{(p-1)DE\ldots M}}{\mathbf{R}^1_{de\ldots m}!\mathbf{R}^2_{de\ldots m}!\ldots\mathbf{R}^\varphi_{de\ldots m}!\left(1+\tau^z_{DE\ldots M}\right)}P^k_{(1)nw}\right].
\end{aligned}
\tag{24}
$$

All these eigenvalue and eigenvector coefficients can be computed using a perturbation algorithm described as follows. With the known changes of the eigenvalues, $\lambda^k_d-\lambda^k$, in Equation (4) and those of the eigenvectors, $\overline{\phi}^k_d-\overline{\phi}^k$, in Equation (5), the perturbation equations at each estimation are generated. The changes of all stiffness parameters are then calculated from these equations using a quasi-Newton optimization method.

In order to validate the accuracy of these results, we compare these perturbation coefficients with those from the general-order perturbation. One can obtain the second-order eigenvalue coefficient from the general-order perturbation (GOP) method as

$$
\lambda^k_{(2)de}=\frac{1}{2!}\overline{\phi}^{kT}\left(\frac{\partial K}{\partial G_d}\overline{z}^k_{(1)e}+\frac{\partial K}{\partial G_e}\overline{z}^k_{(1)d}\right)=\frac{1}{2}\left(\sum_{\substack{a=1\\a\neq k}}^{n}P^k_{(1)ea}\overline{\phi}^{kT}\frac{\partial K}{\partial G_d}\overline{\phi}^{a}+\sum_{\substack{a=1\\a\neq k}}^{n}P^k_{(1)da}\overline{\phi}^{kT}\frac{\partial K}{\partial G_e}\overline{\phi}^{a}\right),
\tag{25}
$$

where $\overline{z}^k_{(1)d}=\sum_{\substack{a=1\\a\neq k}}^{n}P^k_{(1)da}\overline{\phi}^{a}$ is the eigenvector perturbation vector. The second-order eigenvalue coefficient from this method is given by Equation (14). When the indexes are non-repeated, i.e. $d\neq e$, we have $\mathbf{R}^1_{de}!=0!$ and $\tau^e_d=0$, giving

$$\lambda^k_{(2)de} = \frac{1}{2}\left(\sum_{\substack{a=1\\a\neq k}}^{n} P^k_{(1)ea}\overline{\phi}^{kT}\frac{\partial K}{\partial G_d}\overline{\phi}^a + \sum_{\substack{a=1\\a\neq k}}^{n} P^k_{(1)da}\overline{\phi}^{kT}\frac{\partial K}{\partial G_e}\overline{\phi}^a\right). \tag{26}$$

Comparing this with Equation (25), we have validated that both equations give the same results in eigenvalue perturbation coefficients. Equation (25) seems to be more compact. However, it includes the eigenvector perturbation vectors that are more tedious to compute or program than Equation (26), which are reduced in this method.

Moreover, one can proceed to compare the second-order eigenvector perturbation coefficient. Using the second-order eigenvector perturbation coefficient from the GOP method[2] as

$$P^k_{(2)deh} = \frac{1}{2!(\lambda^k - \lambda^h)}\overline{\phi}^{hT}\left\{\left(\frac{\partial K}{\partial G_d}\bar{z}^k_{(1)e} + \frac{\partial K}{\partial G_e}\bar{z}^k_{(1)d}\right) - \left(\lambda^k_{(1)d}M\bar{z}^k_{(1)e} + \lambda^k_{(1)e}M\bar{z}^k_{(1)d}\right)\right\}, \tag{27}$$

where $\bar{z}^k_{(1)d} = \sum_{\substack{a=1\\a\neq k}}^{n} P^k_{(1)da}\overline{\phi}^a$ is the eigenvector perturbation vector. Therefore, one can obtain

$$P^k_{(2)deh} = \frac{1}{2!(\lambda^k - \lambda^h)}\left\{\overline{\phi}^{hT}\frac{\partial K}{\partial G_d}\sum_{\substack{a=1\\a\neq k}}^{n} P^k_{(1)ea}\overline{\phi}^a + \overline{\phi}^{hT}\frac{\partial K}{\partial G_e}\sum_{\substack{a=1\\a\neq k}}^{n} P^k_{(1)da}\overline{\phi}^a - \sum_{\substack{a=1\\a\neq k}}^{n}\left(\lambda^k_{(1)d}\overline{\phi}^{hT}MP^k_{(1)ea}\overline{\phi}^a + \lambda^k_{(1)e}\overline{\phi}^{hT}MP^k_{(1)da}\overline{\phi}^a\right)\right\}. \tag{28}$$

Using the mass normalization equation, we obtain

$$P^k_{deh} = \frac{1}{2(\lambda^k - \lambda^h)}\left\{\overline{\phi}^{hT}\frac{\partial K}{\partial G_d}\sum_{\substack{a=1\\a\neq k}}^{n} P^k_{(1)ea}\overline{\phi}^a + \overline{\phi}^{hT}\frac{\partial K}{\partial G_e}\sum_{\substack{a=1\\a\neq k}}^{n} P^k_{(1)da}\overline{\phi}^a - \left(\lambda^k_{(1)d}P^k_{(1)ea} + \lambda^k_{(1)e}P^k_{(1)da}\right)\right\}. \tag{29}$$

Likewise, the second-order eigenvector coefficient from this method is given by Equation (17). When the indexes are non-repeated, i.e. $d \neq e$, we have $\mathbf{R}^1_{de}! = 0!$ and $\tau^e_d = 0$, giving

$$P^k_{(2)deh} = \frac{1}{2\left(\lambda^k - \lambda^h\right)}\left(\sum_{\substack{a=1\\a\neq k}}^{n} P^k_{(1)ea}\overline{\phi}^{hT}\frac{\partial K}{\partial G_d}\overline{\phi}^a + \sum_{\substack{a=1\\a\neq k}}^{n} P^k_{(1)da}\overline{\phi}^{hT}\frac{\partial K}{\partial G_e}\overline{\phi}^a - \lambda^k_{(1)d}P^k_{(1)eh} - \lambda^k_{(1)e}P^k_{(1)dh}\right). \tag{30}$$

Thus, we found that both equations give exactly the same results. In addition, it is not difficult to illustrate that both equations are also exactly the same for repeated indexes, i.e. $d = e$. The eigenvector coefficient in Equation (30) is more lengthy, but its terms are simplified during the normalization procedure, and it is expressed in lower-order explicit terms, which are more convenient to generate sequentially.

3. Davidon–Fletcher–Powell quasi-Newton approach for optimization of the perturbation equation

The objective in the perturbation algorithm is to estimate the stiffness parameters of the structure so that its eigenparameters from the computational model closely resemble those from the damaged case, $\overline{\Phi}_D = (\lambda^1_D, \overline{\phi}^1_D, \lambda^2_D, \overline{\phi}^2_D, \ldots, \lambda^n_D, \overline{\phi}^n_D)^T$. The algorithm reads in and transforms the eigenparameter of the original computational structure to its master degrees of freedom. Impaction of the work lies on the use of an elastic modulus

as the monitoring parameter, for which not just Young's modulus can be changed but also its physical dimensions, such as width and thickness. This availability is essential in the corrosion detection of lightning poles in an electrical substation in Baltimore city in Maryland [13], where a cross-sectional area of the lightning pole reduced in significant proportion after a long period of outdoor service. Our ultimate goal is to estimate the elastic moduli, $G_d = E_d I / l_e^3$ (where E_d is the Young's modulus of the dth element, I and l_e are its moment of inertia and length respectively), of the structural components that serve as the structural parameters of the system. With the use of explicit perturbation coefficient equations, these coefficients can be constructed progressively from the lower-order coefficients. From the developed methodology, the left-hand sides of the system equations, such as Equations (4) and (5), are $\overline{\phi}_D^k$ and λ_D^k from the simulated data of the damaged case, and the first terms on the right-hand sides of these equations are the eigenparameters of the computational model from previous estimation. In the first estimation, λ^k and $\overline{\phi}^k$ in the system equations are the updated eigenparameters of the undamaged beam. Substituting these coefficients in Equations (4) and (5), the system perturbation equations are formed. In order to optimize the changes to elastic moduli from these large-scale perturbation equations, the DFP quasi-Newton method is established. We use the notations ε_λ^k and $\overline{\varepsilon}_\phi^k$ to denote errors in satisfying the system equations in Equations (4) and (5), respectively. We choose a set of n eigenparameter pairs in the detection process. Let the number of master degrees of freedom of $\overline{\phi}_d^k$ be N_m, $N_m = N$, and $N_m < N$ when we have complete and reduced-order eigenvector measurements, respectively. Hence we establish the weighted eigenparameter perturbation residual objective function as

$$J = \sum_{k=1}^{n} W_\lambda^k (\varepsilon_\lambda^{k(p)})^2 + \sum_{k=1}^{n} W_{\overline{\phi}}^k (\overline{\varepsilon}_\phi^{k(p)})^T (\overline{\varepsilon}_\phi^{k(p)}), \tag{31}$$

where W_λ^k ($k = 1, 2, \ldots, n$) and $W_{\overline{\phi}}^k$ ($k = 1, 2, \ldots, n$) are the weighting factors, and J is a function of $\delta G_d^{(w)}$ when one substitutes the expressions for $\varepsilon_\lambda^{k(p)}$ and $\overline{\varepsilon}_\phi^{k(p)}$ of Equations (4) and (5) into Equation (31). This is an over-determined system, where $n + nN_m > m$, and the DFP quasi-Newton approach is used to determine $\delta G_i^{(w)}$ iteratively. Meanwhile, $J = 0$ (i.e. $\varepsilon_\lambda^{k(p)} = \overline{\varepsilon}_\phi^{k(p)} = 0$) when the optimal solutions are reached. To minimize this objective function at the wth iteration, one can use the updating equation

$$\delta \overline{G}_{(b)}^{(w)} = \delta \overline{G}_{(b-1)}^{(w)} - \alpha_b B_{b-1} \overline{g}_{b-1} \tag{32}$$

to update the variations in the stiffness parameters, where $\delta \overline{G}_{(b)}^{(w)} = (\delta G_{1(b)}^{(w)}, \delta G_{2(b)}^{(w)}, \ldots, \delta G_{m(b)}^{(w)})^T$, $\alpha_b \geq 0$ is the step size, and the gradient vector associated with $\delta \overline{G}_{(b-1)}^{(w)}$ equals $\overline{g}_{b-1} = (\frac{\partial J}{\partial G_1^{(w)}}, \frac{\partial J}{\partial G_2^{(w)}}, \ldots, \frac{\partial J}{\partial G_m^{(w)}})^T$. Note that the subscript b ($b \geq 1$) in all variables in Equation (32) denotes the number of nested iterations. The initial values used are $\delta G_{d(0)}^{(w)} = 0$. The nested iteration is terminated when $\alpha_b \left\| \overline{g}_{b-1} \right\|_\infty < \gamma$, where $\| \cdot \|_\infty$ is the infinity norm and γ is some small constant, or the number of nested iterations exceeds an acceptable number, D.

Due to its successive linear approximations to the objective function, the gradient algorithm may propagate slowly when approaching a stationary point. The DFP quasi-Newton approach provides a remedy to this problem by using essentially quadratic approximation to the objective function near the stationary point. Its iteration scheme is given by Equation (26), where B_{b-1} is an approximation to the inverse of the Hessian matrix used at the bth nested iteration. Initially, we set $\delta G_{d(0)}^{(w)} = 0$ and $B_0 = I$ as the identity matrix. The matrix B_b is updated using the DFP formula:

$$B_b = B_{b-1} + \frac{(\delta \overline{G}_{(b)}^{(w)} - \delta \overline{G}_{(b-1)}^{(w)})(\delta \overline{G}_{(b)}^{(w)} - \delta \overline{G}_{(b-1)}^{(w)})^T}{(\delta \overline{G}_{(b)}^{(w)} - \delta \overline{G}_{(b-1)}^{(w)})^T (\overline{g}_b - \overline{g}_{b-1})} - \frac{[B_{b-1}(\overline{g}_b - \overline{g}_{b-1})][B_{b-1}(\overline{g}_b - \overline{g}_{b-1})]^T}{(\overline{g}_b - \overline{g}_{b-1})^T B_{b-1} (\overline{g}_b - \overline{g}_{b-1})}. \tag{33}$$

The nested iteration is terminated when $\alpha_b \left\| B_{b-1} \overline{g}_{b-1} \right\|_\infty < \gamma$ or the number of iterations exceeds D. The optimization process, including the step-size search procedure, is described below.

3.1. Step-size search procedure

The optimal step size is determined in each nested iteration to minimize the function $J(\delta\mathbf{G}^{(w)}_{(b-1)} - \alpha_b B_{b-1}\overline{g}_{b-1}) = F(\alpha_b)$ with respect to α_b. The search procedure is divided into two phases: (1) initial search to bracket the optimal α_b^*; and (2) golden section search to locate α_b^* within the bracket.

3.2. Initial bracketing

The initial bracketing procedure begins with choosing the starting point $\alpha_1 = 0$ and an initial increment $\Delta > 0$. Then, let $\alpha_2 = \alpha_1 + \Delta$, $F_1 = F(\alpha_1)$, and $F_2 = F(\alpha_2)$. Since for this method, $B_0\overline{g}_0 = I\overline{g}_0 = \overline{g}_0$ and it is along a descent direction of J when Δ is sufficiently small, one has $F_2 < F_1$. Rename 2Δ asΔ, and let $\alpha_3 = \alpha_2 + \Delta$, and $F_3 = F(x_3)$. If $F_3 > F_2$, one should stop and α_b^* is contained in the interval(α_1, α_3). Otherwise, α_2 should be renamed as α_1 and α_3 asα_2, then F_2 becomes F_1 and F_3 becomes F_2. Rename 2Δ as Δ, let $\alpha_3 = \alpha_2 + \Delta$, and $F_3 = F(x_3)$. Compare F_3 and F_2 and repeat the above procedure if $F_3 < F_2$ until $F_3 > F_2$ with the final interval (α_1, α_3) containing α_b^*.

3.3. Golden section search

If $|\alpha_3 - \alpha_2| > |\alpha_2 - \alpha_1|$, define a new point:

$$\alpha_4 = \alpha_2 + 0.382(\alpha_3 - \alpha_2). \tag{34}$$

Otherwise, α_1 should be renamed as α_3 and α_3 as α_1, and then define α_4 using Equation (34). Now, let $F_4 = F(x_4)$. If $F_2 < F_4$, α_4 should be renamed as α_3, then F_4 becomes F_3. Otherwise, rename α_2 as α_1 and α_4 asα_2, then F_2 becomes F_1 and F_4 becomesF_2. Comparing $|\alpha_3 - \alpha_2|$ and $|\alpha_2 - \alpha_1|$, and repeating the above procedure until $|\alpha_3 - \alpha_1| \cdot \left\| B_{b-1}\overline{g}_{b-1} \right\|_\infty < \varepsilon_\alpha$, where ε_α is golden section search accuracy. Then we choose $\alpha_b^* = (\alpha_1 + \alpha_3)/2$. When the b nested search is completed, elastic moduli in this computational model are then updated by

$$G_d^{(w+1)} = G_d^{(w)} + \delta G_d^{(w)}, \tag{35}$$

where $\partial G_d^{(w)}$ is the estimated change of the dth elastic modulus. Note that in each subsequent estimation (i.e. $w \geq 2$), Equations (4) and (5) are modified by replacing elastic moduli $G_d, G_e, \ldots$, and with $G_d^{(w)}, G_e^{(w)}, \ldots$, and $G_z^{(w)}$, respectively, while all the selected eigenparameters and their coefficients are reanalyzed using the fixed–fixed beam model. From the calculated changes of the eigenparameters on the left-hand sides of the resulting perturbation equations, one calculates inversely the change of the elastic modulus $\partial G_d^{(w)}$, and updates the elastic modulus using Equation (35). Two process indicators are used during the estimation process.

1) This process indicator is attained when the total norm of the weighted normalized eigenparameter difference vector drops below dn% of the eigenparameter difference vector (d-norm):

$$\begin{aligned} \|\mathrm{d}\|^{(w_{dn})} &= n_{\overline{\phi}_d} \sum_{i=1}^{n_\phi} W_{\overline{\phi}_d^i} \left\| \frac{\overline{\phi}^{i(w_{dn})} - \overline{\phi}_d^i}{\max\left|\overline{\phi}_d^i\right|} \right\| + \sum_{j=1}^{n_\lambda} W_{\lambda_d^j} \left\| \frac{\lambda^{j(w_{dn})} - \lambda_d^j}{\lambda_d^j} \right\| \\ &\leq \frac{dn}{100} \left(n_{\overline{\phi}_d} \sum_{i=1}^{n_\phi} W_{\overline{\phi}_d^i} \left\| \frac{\overline{\phi}^{i(0)} - \overline{\phi}_d^i}{\max\left|\overline{\phi}_d^i\right|} \right\| + \sum_{j=1}^{n_\lambda} W_{\lambda_d^j} \left\| \frac{\lambda^{j(0)} - \lambda_d^j}{\lambda_d^j} \right\| \right), \end{aligned} \tag{36}$$

where $n_{\overline{\phi}_d^i}$ is the total degrees of freedom of $\overline{\phi}_d^i$, $W_{\overline{\phi}_d^i}$ is the weighting factor of the ith damaged eigenvector, $W_{\lambda_d^j}$ is the weighting factor of the jth damaged eigenvalue, and w_{dn} is the smallest estimation number for which the dn % criterion is reached.

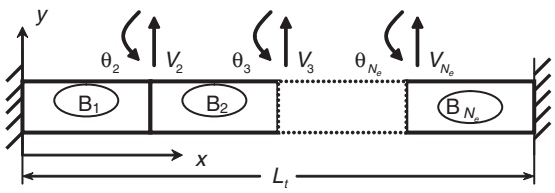

Figure 1. Computational model of odd elements beam with the fixed-fixed boundary condition.

2) This process indicator is attained when the norm of the eigenparameter difference vector drops below *tn*% of the total norm of weighted normalized damaged eigenparameter vector (*t*-norm):

$$\|\mathrm{d}\|^{(w_{tn})} = n_{\overline{\phi}_d} \sum_{i=1}^{n_{\overline{\phi}}} W_{\overline{\phi}_d^i} \left\| \frac{\overline{\phi}^{i(w_{tn})} - \overline{\phi}_d^i}{\max\left|\overline{\phi}_d^i\right|} \right\| + \sum_{j=1}^{n_\lambda} W_{\lambda_d^j} \left\| \frac{\lambda^{j(w_{tn})} - \lambda_d^j}{\lambda_d^j} \right\|$$
$$\leq \frac{tn}{100} \left(n_{\overline{\phi}_d} \sum_{i=1}^{n_{\overline{\phi}}} W_{\overline{\phi}_d^i} \left\| \frac{\overline{\phi}_d^i}{\max\left|\overline{\phi}_d^i\right|} \right\| + \sum_{j=1}^{n_\lambda} W_{\lambda_d^j} \right), \tag{37}$$

where w_{tn} is the smallest estimation number for which the *tn*% criterion is reached. One can note that these process indicators are dimensionless numbers. In order to automate the whole process, the algorithm is established under the MatLab programming platform. It integrates the beam's finite element model, vibration analysis, explicit coefficient generation, perturbation equation establishment, and optimization solver. Its main steps are listed below:

(1) construct the system matrices of the eigenvalue problem for the fixed–fixed beam;
(2) compute the eigenparameters of the damaged and updated beam;
(3) calculate the explicit eigenvalue and eigenvector perturbation coefficients;
(4) set-up the inverse system perturbation equations;
(5) estimate $\delta\overline{G}^{(w)}$ from perturbation equations using the quasi-Newton method;
(6) update the stiffness parameter vector;
(7) repeat steps (1)–(6) iteratively until both process indicators are attained;
(8) plot out the estimation curves of the beam's elastic moduli.

4. Structural damage detection of the fixed–fixed beam

After developing the algorithm, its performance was evaluated through different damaged cases. Random damage is applied to all beam elements, but with the constraint of systematic range (i.e. at the same range) from small to medium to large damage percentages. This type of damage occurs when the beams damage progressively under the external environmental load, such as erosion, lightning, thermal creep, or wind gust. This type of load is applied externally to all surfaces of the structure, giving rise to the systematic rusting, corrosion, or stiffness reduction.

4.1. Computational model of the fixed–fixed beam

To investigate the applicability on different orders of the developed algorithm, various damaged cases are introduced to a fixed–fixed beam model. Although it is a simple beam model, it is already applied to the damage detection of power transmission facilities, such as lightning poles, in the electrical substation.[13] The beam of length $L_t = 0.7\ m$, width $W = 0.0254\ m$, and thickness $H = 0.0031\ m$ has area moment of inertia $I = \frac{1}{12}WH^3 = 6.3058 \times 10^{-11}\ m^4$ and mass density $\rho = 2715\ kg/m^3$. Its finite element model, shown in Figure 1, is used to model its transverse vibration. The beam is divided into N_e elements with the length of each element being $l_e = L_t/N_e$, and there are $N_e + 1$ nodes. With V_d and θ_d denoting the y-translational and

rotational displacements at the dth node ($d = 1, 2, \ldots, N_e + 1$), the displacement vector of the dth element is $\overline{q}_d^e = [V_d, \theta_d, V_{d+1}, \theta_{d+1}]^{\mathrm{T}}$. Using the tensile force F^x, bending force F^y, and torsional moment M^z, the force vector is $\overline{F}_d^e = \left[F_d^x, F_d^y, M_d^z, F_{d+1}^x F_{d+1}^y, M_{d+1}^z\right]^{\mathrm{T}}$. Without loss of generality, y-translational displacement is represented by a cubic Hermite curve with respect to x:[14]

$$V_x = \alpha_1 + \alpha_2 x + \alpha_3 x^2 + \alpha_4 x^3 \tag{38}$$

and rotational displacement $\theta_x$is the derivative of V_x, given by

$$\theta_x = \alpha_2 x + 2\alpha_3 x + 3\alpha_4 x^2. \tag{39}$$

Equations (38) and (39) can be represented in matrix form:

$$\left\{ \begin{array}{c} V_x \\ \theta_x \end{array} \right\} = \left[\begin{array}{cccc} 1 & x & x^2 & x^3 \\ 0 & 1 & 2x & 3x^2 \end{array} \right] \left\{ \begin{array}{cccc} \alpha_1 & \alpha_2 & \alpha_3 & \alpha_4 \end{array} \right\}^T = \left[\begin{array}{c} S_V \\ S_\theta \end{array} \right] \overline{\alpha}^e = S\overline{\alpha}^e. \tag{40}$$

This is the displacement equation of any point within the element. From this relation, one can obtain the start- and end-point equations at $x = 0, l_e$, respectively:

$$\left\{ \begin{array}{c} V_d \\ \theta_d \\ V_{d+1} \\ \theta_{d+1} \end{array} \right\} = \left[\begin{array}{cccc} 1 & 0 & 0 & 0 \\ 0 & 1 & 0 & 0 \\ 1 & l_e & l_e^2 & l_e^3 \\ 0 & 1 & 2l_e & 3l_e^2 \end{array} \right] \left\{ \begin{array}{cccc} \alpha_1 & \alpha_2 & \alpha_3 & \alpha_4 \end{array} \right\}^T = A\{\alpha\}, \tag{41}$$

where A is the displacement matrix of the end points. Using its inverse, the shape function vector is obtained as

$$\overline{N}_e = S_V A^{-1} = \frac{1}{l_e^3} \left\{ \begin{array}{cccc} l_e^3 - 3x^2 l_e + 2x^3 & x l_e^3 - 2x^2 l_e^2 + x^3 l_e & 3x^2 l_e - 2x^3 & -x^2 l_e^2 + x^3 l_e \end{array} \right\}. \tag{42}$$

By the virtue work principle,[14] the element mass matrix is obtained by substituting $\overline{N}_e$ as

$$M_d^e = \int_0^{l_e} \rho WH \overline{N}_e^T \overline{N}_e dx = \frac{\rho WHl_e}{420} \left[\begin{array}{cccc} 156 & 22l_e & 54 & -13l_e \\ 22l_e & 4l_e^2 & 13l_e & -3l_e^2 \\ 54 & 13l_e & 156 & -22l_e \\ -13l_e & -3l_e^2 & -22l_e & 4l_e^2 \end{array} \right]. \tag{43}$$

In addition, the strain at arbitrary point (x, y) is given by

$$\begin{aligned} \overline{\varepsilon}_d^e &= -y \frac{\partial^2 S_V^e}{\partial x^2} \overline{q}_d^e \\ &= \left[\frac{6y}{l_e^2} - \frac{12yx}{l_e^3} \ \frac{4y}{l_e} - \frac{6yx}{l_e^2} \ \frac{-6y}{l_e^2} + \frac{12yx}{l_e^3} \ \frac{2y}{l_e} - \frac{6yx}{l_e^2} \right] \overline{q}_d^e = B_d^e \overline{q}_d^e, \end{aligned} \tag{44}$$

where B_d^e is the element strain matrix, which depends only on the geometry of the element. According to the virtue work principle, the force vector is

$$\overline{F}_d^e = \int_{-\frac{W}{2}}^{\frac{W}{2}} \int_{-\frac{H}{2}}^{\frac{H}{2}} \int_0^{l_e} B_d^{eT} E_d B_d^e \ dxdydz \cdot \overline{q}_d^e = K_d^e \overline{q}_d^e, \tag{45}$$

where K_d^e is the element stiffness matrix. From this equation, K_d^e is determined as

$$K_d^e = \frac{E_d I}{l_e^3} \left[\begin{array}{cccc} 12 & 6l_e & -12 & 6l_e \\ 6l_e & 4l_e^2 & -6l_e & 2l_e^2 \\ -12 & -6l_e & 12 & -6l_e \\ 6l_e & 2l_e^2 & -6l_e & 4l_e^2 \end{array} \right]. \tag{46}$$

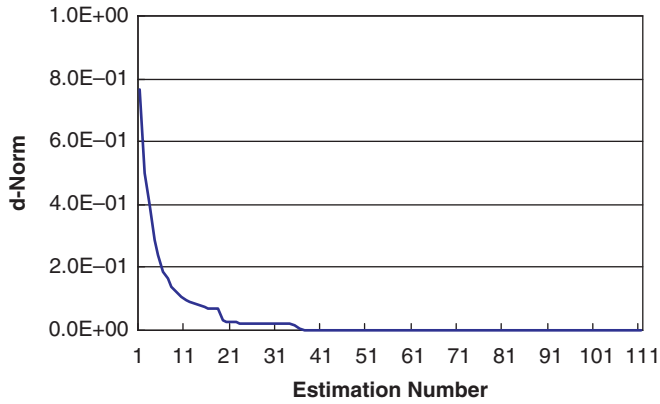

Figure 2. Case 5o1_rs: first-order estimation d-norm of the five elements beam with systematic small-percentage random damage.

Utilizing this matrix, one can extract out the constant term $G_d = E_d I / l_e^3$, which is the elastic modulus of the beam element. Its value in a healthy beam element is $G_h = 8.118 \times 10^2$ N/m. Moreover, this validated the assumption that the stiffness matrix is the first order of G_d as discussed in Equation (3). Small, medium, and large-percentage damages, which correspond to the reduction in elastic moduli of 0–30%, 30–60%, and 60–90%, respectively, are simulated on the beam. Using the standard assembly process yields the system mass matrix of Equation (1), i.e. $M = \sum_{d=1}^{N_e} M_d^e$. For the initial element at $d = 1$, the 4×4 element mass matrix of Equation (43) is assembled to the system mass matrix at degrees of freedom 1 to 4. At the intermediate element ($d = i$), the element mass matrix is assembled to the system mass matrix at degrees of freedom $2i - 1$ to $2i + 2$. For the final element at $d = N_e$, the element mass matrix is assembled to the degrees of freedom $2N_e - 1$ and $2N_e + 2$. Similarly, the system stiffness matrix is assembled as $K = \sum_{d=1}^{N_e} K_d^e$ using Equation (46), where its dimensions are $2(N_e + 1) \times 2(N_e + 1)$. Now we should set the boundary conditions for this fixed–fixed beam. By constraining the translational and rotational displacements, degrees of freedom 1 and 2 are eliminated at the first node, while degrees of freedom $2N_e + 1$ and $2N_e + 2$ are eliminated at the $(N_e + 1)$th node. Thus, the M and K matrices are generated with dimensions $2(N_e - 1) \times 2(N_e - 1)$, where $2(N_e - 1)$ is the degree of freedom of the system. The displacement vector of the system containing the unconstrained nodes becomes the eigenvector $\overline{\phi}^k = [V_2, \theta_2, V_3, \theta_3, \ldots, V_{N_e}, \theta_{N_e}]^T$, which is obtained by solving the eigenvalue problems in Equation (1) or (2). In order to evaluate the performances of different order algorithms, various levels of random damages are introduced to the modular beam with five elements from cases 5o1_rs to 5o2_rl to establish its systematic random damage cases. For small-percentage damaged cases, the damaged ranges are 0–30% for small percentages, 30–60% for medium percentages, and 60–90% for large percentages. Nevertheless, it is uniform random distributed. Hence,

$$G_d = G_h (D_r + 0.3 \cdot \Theta) \, d = 1, 2, \ldots, m, \tag{47}$$

where D_r is the damage range index, Θ is the $[0, 1]$ uniform random number, and other terms are defined as before.

4.2. Small-percentage systematic damage

At first, using the first-order algorithm for the small-percentage damages, $D_r = 0.7$ with $W_{\overline{\phi}_d^i} = 1$, $W_{\lambda_d^j} = 0.2$, and $dn = 1$. The d-norm drops rapidly from 7.64×10^{-1} to 1.06×10^{-1} in ten estimations (Figure 2), then it reaches the cliff around estimation 18 in the first region. It remains at a flat plateau until estimation 35 and drops to a 1% d-norm level at estimation 36 in the second region. Finally, it remains at the flat region until t-norm indicator 10^{-4}% t-norm, $tn = 10^{-4}$, is reached at estimation 112. From the estimation chart of

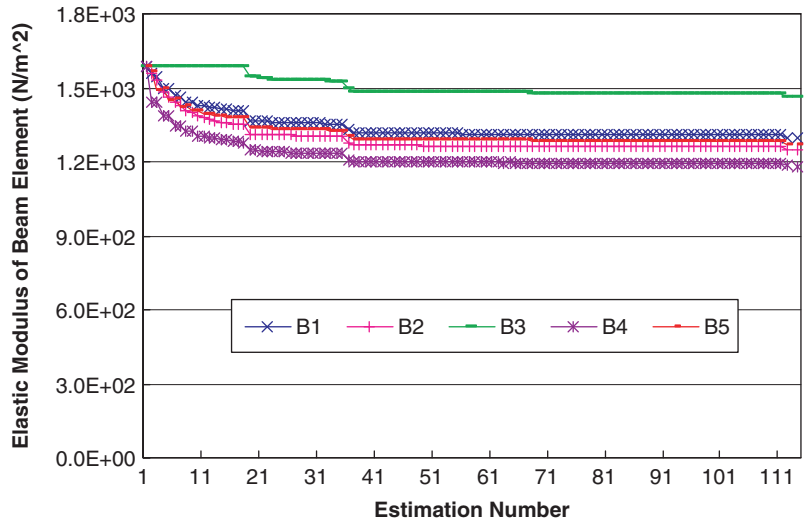

Figure 3. Case 5o1_rs: first-order damage detection curves of the five elements beam with systematic small-percentage random damage (0.7–1.0 $E_h I/l_e^3$).

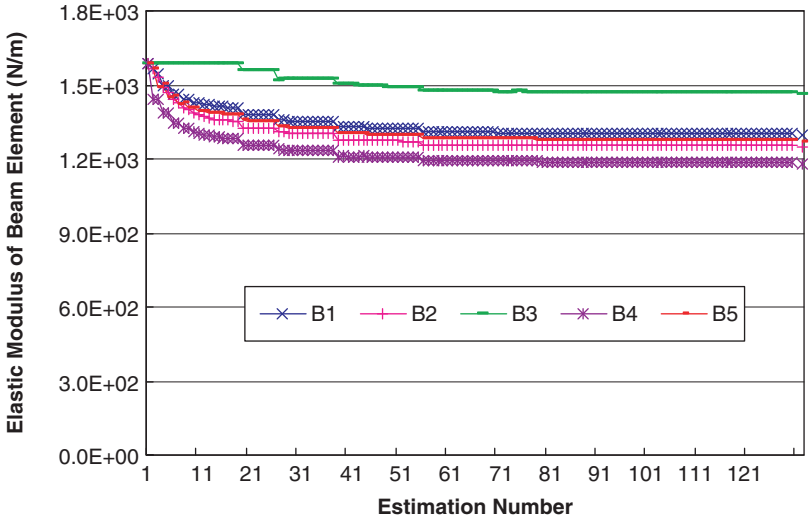

Figure 4. Case 5o2_rs: second-order damage detection curves of the five elements beam with systematic small-percentage random damage (0.7–1.0 $E_h I/l_e^3$).

Figure 3, one can observe that elements B1, B2, B4, and B5 drop regularly in the first region, then they drop stepwise, together with element B3, until estimation 36 in the second region. Afterwards, they drop one after the other until estimation 112.

For the second-order algorithm, the d-norm drops rapidly from 2.97×10^{-1} to 4.44×10^{-3} around the cliff at estimation 21 in the first region. Then it remains at the flat region until 1% d-norm level at estimation 27. Finally, it remains at the flat region until t-norm indicator 10^{-4}% t-norm, $tn = 10^{-4}$, is reached at estimation 131. From the estimation chart in Figure 4, one can observe that elements B1, B2, B4, and B5 drop regularly in the first region, then they drop stepwise with element B3 until estimation 20 in the second region. In these plateau regions, they drop stepwise one after the other until estimation 131. In the GOP method[2] including the kth term, the convergence patterns are more gradual and decrease consistently. Meanwhile, the plateau region is shortened to estimation 101.

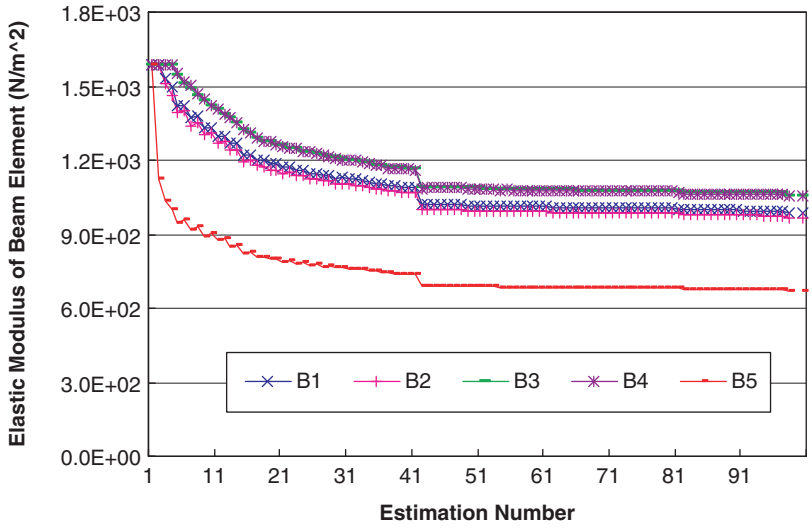

Figure 5. Case 5o1_rm: first-order damage detection curves of the five elements beam with systematic medium-percentage random damage (0.4–0.7 $E_h I/l_e^3$).

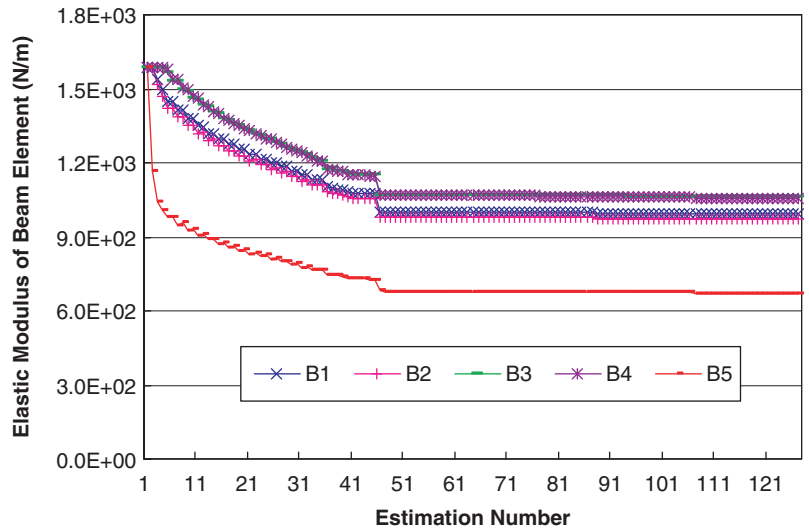

Figure 6. Case 5o2_rm: second-order damage detection curves of the five elements beam with systematic medium-percentage random damage (0.4–0.7 $E_h I/l_e^3$)

4.3. Medium-percentage systematic damage

Secondly, using the first-order algorithm in detecting medium-percentage damages, $D_r = 0.4$, the d-norm drops rapidly from 2.55 to 1.04 at the cliff around estimation 38 in the first region. Then it remains at the flat region until estimation 98, where the t-norm indicator is reached. From the estimation chart in Figure 5, one can observe that all elements drop regularly in the first region, then they drop stepwise together in the second region. In this plateau region, they drop one after the other until estimation 98.

For the second-order algorithm, the d-norm drops rapidly from 0.972 to 7.94×10^{-4} at the cliff around estimation 47 in the first region, and it remains at the flat region until estimation 128, where the t-norm indicator is reached. From the estimation chart in Figure 6, one can observe that elements B2 and B3 remain at the upper bound up to the fifth estimations, then they drop regularly with elements B1, B2, and B5 in the first region. Afterwards, they remain at the plateau region basically and drop to the ultimate levels at estimation 128. Similar pattern can be observed in the GOP method including the kth term, but the plateau region is shortened to estimation 69.

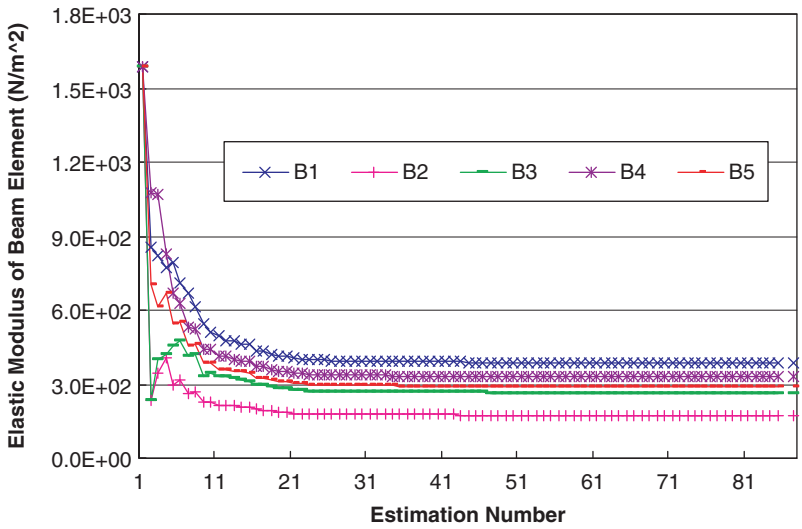

Figure 7. Case 5o1_rl: first-order damage detection curves of the five elements beam with systematic large-percentage random damage (0.1–0.4 $E_h I/l_e^3$)

4.4. Large-percentage systematic damage

Thirdly, the first-order algorithm is applied to the large-percentage random damages ($D_r = 0.1$) with the estimation chart as in Figure 7. The d-norm drops rapidly from 228 to 8.85 at the first estimation. Then it rises and drops in the first hill region until estimation nine where the 1% d-norm level is attained. Afterwards, it remains at the second plateau region until estimation 84, where the t-norm indicator is reached. From the estimation chart, all elements interact vigorously in the hill region, then they drop gradually and stepwise one after the other until estimation 84.

For the second-order algorithm, the d-norm drops rapidly from 24.2 to 1.59 in four estimations at the first region, then it drops regularly to 1% d-norm level at estimation nine. Afterwards, it remains at the third plateau region until the t-norm indicator is attained at estimation 48. From the estimation chart in Figure 8, all elements interact vigorously initially in the first region, then they drop gradually in the second region. Afterwards, they drop stepwise one by one until estimation 48, where the t-norm indicator is attained. For the GOP method including the kth term, nearly same convergence patterns are observed. However, the t-norm indicator is attained later at estimation 52.

Firstly in the order comparison, for large-percentage damages, the convergence of the second-order algorithm is more effective for the t-norm indicator. Moreover, in medium-percentage damaged cases, the convergences of the first-order algorithm are much faster for both indicators. Furthermore, for small-percentage damages, the convergences of the second-order algorithm are slightly more effective for both indicators.

Secondly in the method comparison, in small-percentage damages, the convergence of the GOP method is more effective for the t-norm indicator. Meanwhile, the GOP method is much faster for the t-norm convergence in medium-percentage damages. However, for large-percentage damages, convergence of this method is slightly more effective for the t-norm indicator.

4.5. Damage detection of the seven and nine elements beam

As illustrated in Table 1, for the seven elements medium-percentage damages, the second-order algorithm (estimation 53) converges significantly faster to the 1% d-norm than the first-order algorithm (estimation 89). Meanwhile in the t-norm indicator, the first-order algorithm (estimation 393) converges slower than the second-order algorithm (estimation 289). It is interesting to note that the starting healthy value of the beam varies according to the element number. This is explained by the element length being the total length divided by the element number, i.e. $l_e = L_t/N_e$. From Figure 9, all elements drop regularly to estimation 25 where the

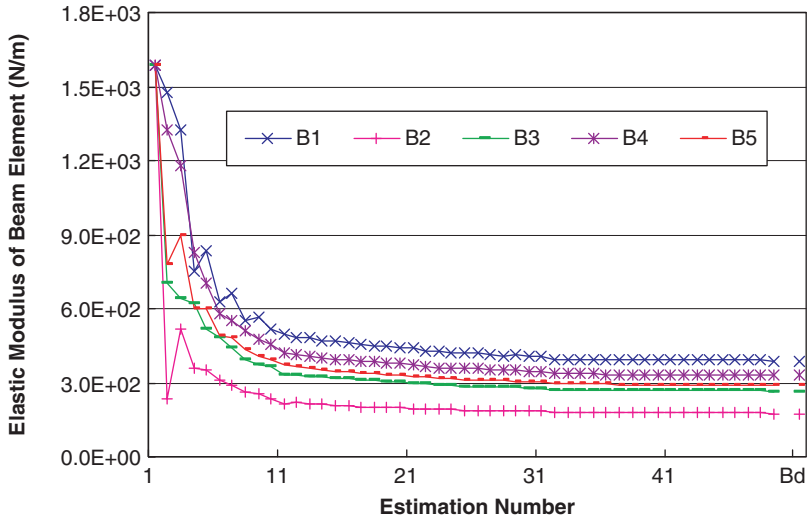

Figure 8. Case 5o2_rl: second-order damage detection curves of the five elements beam with systematic large-percentage random damage (0.1–0.4 $E_h I/l_e^3$).

Table 1. Convergence analysis of seven and nine elements beam damage detection.

	Perturbed method		GOP	
Case	d-norm	t-norm	d-norm	t-norm
7o1_rm	89	393	89	393
7o2_rm	53	289	31	249
9o1_rs	277	301	277	301
9o1_rs	33	109	48	127

cliff region occurs, then they drop stepwise to estimation 68 where the second cliff region is experienced. Afterwards, they propagate in the plateau region where the desired solutions are achieved. As the number of beam elements increases, the order arrangement of their magnitudes requires more estimations in the initial regions. From Figure 6, one can observe that the order arrangement becomes stable in five estimations for the five elements beam, while it takes 25 estimations for the seven elements beam in Figure 9. Moreover, the complexity of the eigenvectors increases, with the element and node numbers leading to more rigorous mode-shifting effects. Thus, more stepwise drops are involved in the arrangement process. In the first-order algorithms for both methods, perturbation coefficients are not constructed from the basic vectors of all used eigenvectors, hence there is no difference for the convergence patterns, as revealed in Table 1.

Now for nine elements small-percentage damages, stepwise drops of the second-order algorithm occur at smaller numbers of estimations than those of the first-order algorithm. Moreover, the 1% d-norm is attained at a smaller estimation number (33), while the t-norm indicator is reached at the smaller number for the second-order algorithm (estimation 61) than the first-order algorithm (estimation 277). One can observe from the estimation chart (Figure 10) of the second-order algorithm that all beam elements drop regularly toward the cliff region at estimation 13. Afterwards, they propagate in the plateau region irregularly until the t-norm indicator is attained at estimation 112. Considering the Hessian matrix, a small change in $\delta\overline{G}_{(b-1)}^{(w)}$ leads to a large change in $\overline{g}_{b-1}$. This explains the extra-low convergent rate, particularly when the change in $\overline{g}_{b-1}$ is small. On the other hand, as the divider includes the inverse Hessian matrix of the previous iteration, this causes numerical instability during the estimation process or a singularity that results in B_{b-1}. Thus, this leads to the extra-low value in the α_b search. Combining these two factors, the convergent rate is lower, leading to flattening behavior in the latter regions of the refinement process.

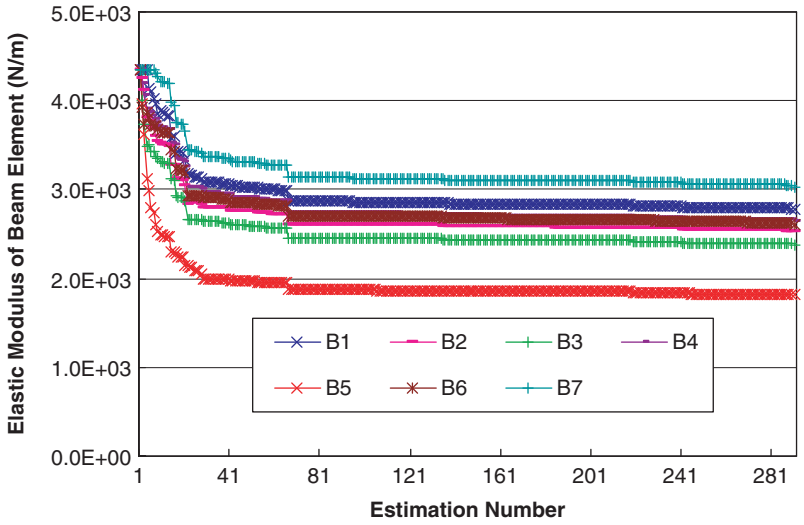

Figure 9. Case 7o2_rm: second-order damage detection curves of the seven elements beam with systematic medium-percentage random damage (0.4–0.7 $E_h I/l_e^3$).

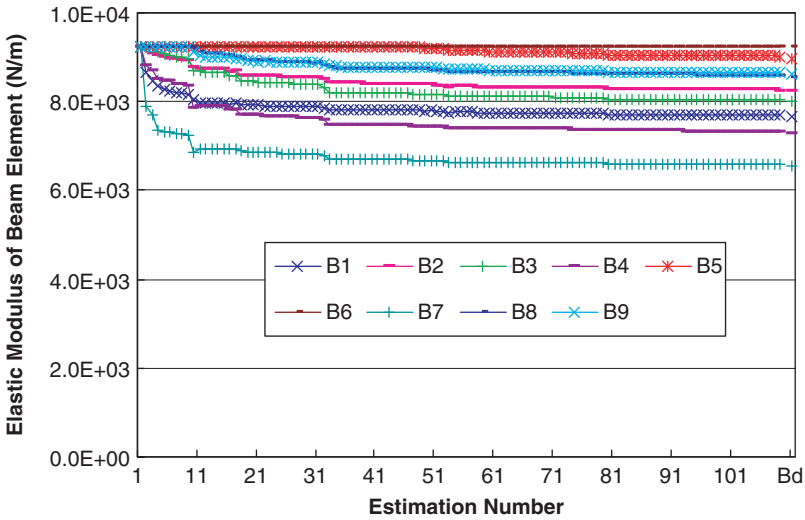

Figure 10. Case 9o2_rs: second-order damage detection curves of the nine elements beam with systematic small-percentage random damage (0.7–1.0 $E_h I/l_e^3$).

5. Conclusion

Using the perturbed eigenvalue problem only, the structural damage detection algorithm was formulated. At first by introducing the perturbed eigenvector and eigenvalue, their non-kth perturbation coefficients were derived explicitly. By comparing these perturbation coefficients with those generated from the GOP method, their correctness is proven. The form of eigenvector coefficient from this method is more lengthy, but its structure is more systematic through the normalization procedure. Moreover, higher-order terms are generated from lower-order explicit terms, which is more direct and convenient.

Secondly, these equations were solved by the DFP quasi-Newton method. Automated damage detection algorithm for the odd elements beam was programmed. In small- and large-percentage damages, the convergence of the second-order algorithm is more effective for the t-norm indicator. Meanwhile, in medium-percentage damaged cases, the convergences of the first-order algorithm are faster for both indicators. By comparing both methods, in small-percentage damages, the convergence of the GOP method is more effective

for the *t*-norm indicator. Meanwhile, the GOP method is much faster for the *t*-norm convergence in medium-percentage damages. However, for large-percentage damages, *t*-norm convergence of this method is slightly more effective.

Thirdly, for seven and nine elements beam cases, the second-order algorithm converges faster both in 1% *d*-norm and 10^{-4}% *t*-norm. These cases reveal that the efficiency of the damage detection process increases with the order of the algorithm. Further investigation needs to be carried out to establish the relationships between higher-order algorithms and their convergences.

5.1. Funding

This work was supported by the National High Technology Research and the Development Program of China (863 Program; grant number 2007AA04Z403) and the Jinchuan Group Ltd (grant number H04010801W080421).

5.2. Conflict of interest

The author declared no conflicts of interest with respect to the authorship and/or publication of this article.

Acknowledgements

The authors gratefully thank Dr William Wood of the University of Maryland Baltimore County for the optimization algorithm development of this work.

References

[1] Wilkenson, JH. *The Algebraic Eigenvalue Problem*. Oxford: Clarendon Press, 1965.
[2] Wong, CN, Zhu, WD, and Xu, GY. On an iterative general-order perturbation method for multiple structural damage detection. *J Sound Vib* 2004; 273: 363–386.
[3] Wong, CN, Chen, JC, and To, WM. Eigenparameter perturbation method for structural damage detection. In: *37th AIAA/ASME/ASCE/AHSASC Structural Forum 76-ASF-9*, Salt Lake City, UT, 1996, pp.658–667.
[4] Chen, SH. Matrix perturbation method of degenerate vibration systems. *J Jilin University Tech* 1981; 4: 11–15.
[5] Hu, HC. *Natural Vibration Theory of Multi-degree-of-freedom Structures*. Beijing: China Science Press, 1987, pp. 17–24.
[6] Chen, SH, Liu, ZS, Shao, CS, and Zhao, YQ. Perturbation analysis of vibration modes with close frequencies. *Comm Numer Meth Eng* 1993; 9: 427–438.
[7] Wanxie, Z, and Gengdong, C. Second-order sensitivity analysis of multimodal eigenvalues and related optimization techniques. *J Struct Mech* 1986; 14: 421–436.
[8] Wicher, J, and Nalecz, AG. Second order sensitivity analysis of lumped mechanical systems in the frequency domain. *Int J Numer Meth Eng* 1987; 24: 2357–2366.
[9] Ryland II, G, and Meirovitch, L. Response of vibrating systems with perturbed parameters. *J Guid Contr* 1980; 3: 125–131.
[10] Kan, CL, and Chopra, AK. Elastic earthquake analysis of torsionally coupled multistorey buildings. *Earthquake Eng Struct Dynam* 1977; 5: 395–412.
[11] Kan, CL, and Chopra, AK. Elastic earthquake analysis of a class of torsionally coupled building. *J Struct Div* 1977; 103(4): 821–838.
[12] Tsicnias, TG, and Hutchinson, GL. A note on the perturbation analysis of the mode shapes of torsionally coupled buildings. *Earthquake Eng Struct Dynam* 1982; 10: 171–174.
[13] Zhu, WD, Wong, CN, and Xu, GY. *Iterative Method to Detect Structural Damage Using Vibration Characteristics*. Technical report 10-2003, Baltimore Gas and Electric Corporation, 2003.
[14] Zhang, E. *Modern Design Theory and Method*. Beijing: Science Press, 2007, pp. 127–136.